Applied Catalysis B: Environmental 217 (2017) 48–56

Contents lists available at ScienceDirect

Applied Catalysis B: Environmental

journal homepage: www.elsevier.com/locate/apcatb

Defect engineered Ta_2O_5 nanorod: One-pot synthesis, visible-light driven hydrogen generation and mechanism

Xin Yu[a,b], Wei Li[a], Zhonghua Li[b,*], Jiawen Liu[c,*], Pingan Hu[b,*]

[a] School of Chemistry and Chemical Engineering, Harbin Institute of Technology, Harbin 150001, PR China
[b] Key Laboratory of Microsystems and Microstructures Manufacturing, Ministry of Education, Harbin Institute of Technology, Harbin 150001, PR China
[c] Key Laboratory for Photonic and Electronic Bandgap Materials, Ministry of Education, Harbin Normal University, Harbin 150025, PR China

ARTICLE INFO

Article history:
Received 19 December 2016
Received in revised form 17 April 2017
Accepted 7 May 2017
Available online 8 May 2017

Keywords:
Self-doped Ta_2O_5 nanorod
Semiconductor
Visible-light photocatalysis
Hydrogen production

ABSTRACT

Visible-light photocatalysis of the typical wide band gap semiconductor was often thought to be challenge and focus in the field of solar energy conversion. Hence, it was of great significance for wide band conductors to harvest visible light using photocatalysis technology. In this experiment, we successfully synthesized novel Ta^{4+} doped Ta_2O_5 nanorod by facile one-pot vapor hydrolysis method, and Ta^{4+} species was confirmed by XPS and EPR technology. The as-prepared Ta_2O_5 nanorod displayed amazing visible light absorption from 400 to 800 nm and visible light photocatalytic activity for hydrogen production, and the estimated band gap of Ta_2O_5-180, Ta_2O_5-200, Ta_2O_5-220 and Ta_2O_5-240 catalysts were about 2.93, 2.83, 2.75 and 2.53 eV, much lower than that of commercial Ta_2O_5 (3.88 eV). And the specific surface area of the self-doped Ta_2O_5 catalyst could reach up to 237.89 $m^2\,g^{-1}$ with the typical mesoporous structure. It was noteworthy that the self-doped Ta_2O_5 nanorod displayed inspiring visible light photocatalytic activity for hydrogen production, which could reach up to 23.35 $\mu mol\,g^{-1}\,h^{-1}$, while commercial Ta_2O_5 showed no visible light activity, mainly due to the formation of Ta^{4+} species in the as-prepared Ta_2O_5 nanorod. Besides, the self-doped Ta_2O_5 catalyst showed UV light photocatalytic activity of 10.17×10^3 $\mu mol\,g^{-1}\,h^{-1}$ and the highly enhanced simulated sunlight photocatalytic activity of 356.68 $\mu mol\,g^{-1}\,h^{-1}$ for hydrogen production, which were much higher than those of commercial Ta_2O_5. It was the formation of the Ta^{4+} species, high specific surface area, high crystallization and mesoporous structure that highly enhanced the UV light and simulated sunlight photocatalytic activity of the self-doped Ta_2O_5 nanorod. Finally, possible mechanism of the visible-light photocatalysis of the self-doped Ta_2O_5 nanorod for hydrogen production was also proposed in detail.

1. Introduction

Semiconductor photocatalysis is believed to be one of the most promising technologies for solar energy to be converted into chemical energy to solve the energy and environment problem [1–5]. Since Fujishima and Honda first discovered the water splitting phenomenon on the TiO_2 electrode in 1972 [6], researches of semiconductor photocatalysis on hydrogen production and CO_2 reduction had been carried out for utilization of solar energy [7–9], such as TiO_2 [10,11], Ta_2O_5 [3,12] and CeO_2 [13,14], etc. Hydrogen energy was generally considered to be a new type of efficient and environmental friendly energy [15,16]. And thus, it seemed feasible and inspiring to obtain hydrogen energy using semiconductor photocatalysts from water decomposition [17,18]. However, there are still some disadvantages for semiconductor photocatalysts nowadays, such as the low photocatalytic activity and limited spectrum response range, especially for the wide band gap semiconductors [19–23]. And thus, it was highly expected for the typical wide band gap semiconductor to have excellent visible-light response using photocatalysis technology [24–27].

Tantalic oxide (Ta_2O_5) is a typical wide band gap semiconductor (~3.9 eV) with high dielectric constant and excellent photoelectric property [3,28,29]. And thus, Ta_2O_5 semiconductor does not response to visible light. Nevertheless, the conduction band minimum of Ta_2O_5 was reported to be about −0.17 eV [30], which was more negative than the redox potentials of H^+/H_2 (0 eV) [30]. And thus, it is possible for Ta_2O_5 semiconductor to be applied for hydrogen production according to the thermodynamics theory [3,31–33]. Until now, many kinds of Ta_2O_5 photocatalysts with different morphologies, including Ta_2O_5 sphere [34], Ta_2O_5

* Corresponding authors.
E-mail addresses: lizh@hit.edu.cn (Z. Li), jiawenliu86@163.com (J. Liu), hupa@hit.edu.cn (P. Hu).

http://dx.doi.org/10.1016/j.apcatb.2017.05.024
0926-3373/

nanotube [35] and so on, have been prepared for photocatalytic hydrogen production. However, it was still of great challenge for wide band gap Ta_2O_5 to have visible-light response because of its typical wide band gap (~3.9 eV). Until now, there were only some researches about UV (λ > 200 nm) or simulated sunlight (λ > 320 nm) photocatalytic activity of Ta_2O_5 for hydrogen production to be reported [3,35,36]. Guo's group [37] successfully synthesized crystalline mesoporous Ta_2O_5 by one-pot soft templating method using P123, and the highest photocatalytic activity for hydrogen production was 1.456 mmol g^{-1} h^{-1} under UV irradiation, much higher than that of commercial Ta_2O_5. Besides, guan's group [38] successfully fabricated fluorinated and naked Ta_2O_5 single crystalline nanorods with a UV photocatalytic activity for hydrogen production of ~910 μmol g^{-1} h^{-1} and a specific surface area of 15.76 m^2/g, also much higher than those of commercial Ta_2O_5. And thus, the mesoporous structure and high crystallinity were contributing to promote the photocatalytic activity for hydrogen production of Ta_2O_5 catalysts. Much efforts has been made to extend the spectrum response range and increase the crystallinity and specific surface areas of Ta_2O_5 photocatalysts [36]. However, the visible-light photocatalytic activity of Ta_2O_5 catalyst for hydrogen production has not been reported until now. In general, the effects of Ta^{4+} self-doping (oxygen vacancy defects) in Ta_2O_5 photocatalyst is generally considered to contribute to visible-light response of Ta_2O_5, which would form new defect energy level straddling the valence band maximum and conduction band minimum of Ta_2O_5 and effectively benefit the band gap of Ta_2O_5 with intriguing visible-light response. Recently, Zhang and huang's group [12] fabricated new Ta_2O_5 nanowires with disordered shells and abundant defects via aluminum reduction, and the photocatalytic hydrogen production rate was as highly as 2.05 mmol g^{-1} h^{-1} under 300 W Xe lamp irradiation, showing highly enhanced hydrogen production activity in comparison to that of pristine Ta_2O_5. And therefore, visible-light photocatalysis for hydrogen production of the self-doped Ta_2O_5 nanorod is intriguing and highly expected nowadays.

In this work, novel Ta^{4+} self-doped Ta_2O_5 nanorod was successfully synthesized by vapor hydrolysis reaction at different temperatures. We investigated the UV light, simulated sunlight and visible-light photocatalytic activity of the self-doped Ta_2O_5 nanorod for hydrogen production, respectively, which showed great advantages in comparison to those of commercial Ta_2O_5 powder. Finally, the formation procedure and possible visible-light photocatalysis mechanisms of the self-doped Ta_2O_5 nanorod for hydrogen production were also proposed in detail.

2. Experimental

2.1. Preparation of the self-doped Ta_2O_5 nanorod

All the raw materials in this experiment were commercially available and used directly without any purification. The Ta^{4+} self-doped Ta_2O_5 nanorod was prepared by facile vapor hydrolysis reaction. In a typical procedure, 8 mL distilled water was added into a Teflon line, and 0.30 g $Ta(C_2H_5O)_5$ was dissolved in 6 mL NH_4F-ethylene glycol solution (0.1 mol L^{-1}) in an inner container and stirred for about 30 s, then the mixture was transferred into the Teflon line. After sealing the autoclave, the vapor hydrolysis reaction was carried out at 180, 200, 220 and 240 °C for 20 h to prepare self-doped Ta_2O_5 nanorod, respectively. After being cooled to room temperature by water, washed with ethanol for several times and dried in an oven at 60 °C for 24 h, the self-doped Ta_2O_5 nanorod was obtained. The self-doped Ta_2O_5 catalysts prepared at 180, 200, 220 and 240 °C were denoted by Ta_2O_5-180, Ta_2O_5-200, Ta_2O_5-220 and Ta_2O_5-240, respectively. Scheme 1 displayed the schematic illustration of the formation procedure of the crystallized self-doped Ta_2O_5 nanorod.

2.2. Characterization

The morphology of the as-prepared self-doped Ta_2O_5 nanorod was investigated by Transmission electron microscope (TEM) and HRTEM (Tecnai, G2F30) at 300 kV. The crystal structure was studied by X-ray diffraction pattern (XRD) (Panalytical Corporation, Empyrean) with Cu Kα radiation (λ = 0.15406 nm). The element chemical states were studied on an X-ray photoelectron spectroscopy (XPS) (Thermo Fisher Scientific, ESCALAB 250Xi). The UV–vis diffuse reflectance absorption spectra were measured by the double-beam ultraviolet-visible absorption spectrophotometer (Beijing's general instrument co., LTD, TU-1900) using $BaSO_4$ as the reference standard. The Nitrogen adsorption-desorption isotherms were measured on a Nitrogen adsorption analyzer (Quantachrome corporation, NOVA 2000E). The uncoupled electron properties were investigated on an Electron paramagnetic resonance (EPR) at 90 K (Bruker Corporation, A300-10/12) with a mount of 0.10 g catalyst. The surface photo-induced charge kinetic behavior was studied on a Surface photovoltage spectroscopy (PL-SPS/IPCE1000, Beijing perfectlight Co., Ltd., China) at room temperature. The electrochemical impendence spectra was determined by a CHI660D electrochemical working station (shanghai, Chen hua) with electrodes of the catalysts, Pt wire electrode and Ag/AgCl electrode were as the working electrode, counter electrode and reference electrode in 0.1 M Na_2SO_4 solution. The working electrode was prepared by electrophoretic deposition with a small amount of $Mg(NO_3)_2$ (0.0074 g) for 6 min at a 50 V direct-current voltage [39].

2.3. Photocatalytic hydrogen production

We investigated the photocatalytic activity of the self-doped Ta_2O_5 nanorod for hydrogen production under UV light, simulated sunlight and visible light irradiation in 100 mL methanol aqueous solution (20 vol.%) in detail. The photocatalytic hydrogen production experiments were carried out in a sealed gas circulation and evacuation system (LabSolar- III AG, Beijing PerfectLight Co., Ltd., China). The reactor was placed under the Xe lamp. In a typical procedure, 0.05 g self-doped Ta_2O_5 catalyst with 2 wt% Pt cocatalyst was added in the methanol aqueous solution and treated by ultrasound for 30 min to obtain a well-dispersed mixture. Then the mixture was transferred into the reactor with a quartz cover. After sealing the reactor and the pressure being evacuated to about −0.1 MPa, the reactor was then irradiated by a 300W Xe lamp (PLS SXE300C, Beijing PerfectLight Co., Ltd., China) for 60 min to in suit photodeposite $H_2PtCl_6{\cdot}(H_2O)_6$ onto the self-doped Ta_2O_5 nanorod with a current of 20 A and continuously stirring. After Pumping the H_2 produced in photodeposition process and the pressure being evacuated to about −0.1 MPa again, the photocatalytic hydrogen production test was carried out with continuous stirring. The UV light hydrogen production test was carried out under a 300W Xe lamp (PLS SXE300C) for 60 min with a current of 20 A, and the simulated sunlight hydrogen production activity test was also carried out on a 300 W Xe lamp (MicroSolar 300, Beijing PerfectLight Co., Ltd., China) for 180 min with a current of 20 A. The visible-light hydrogen production test was carried out on a 300 W Xe lamp (MicroSolar 300) with a 400 nm cut-off filter for 180 min with a current of 20 A. The generated hydrogen was analyzed by gas chromatography (Techcomp, 7890 II) with Ar carrier gas and a molecular sieve 5 Å TCD detector.

3. Result and discussion

Fig. 1 showed the TEM and HRTEM images of the self-doped Ta_2O_5-220 nanorod. As shown in Fig. 1 (a), the as-prepared Ta_2O_5-

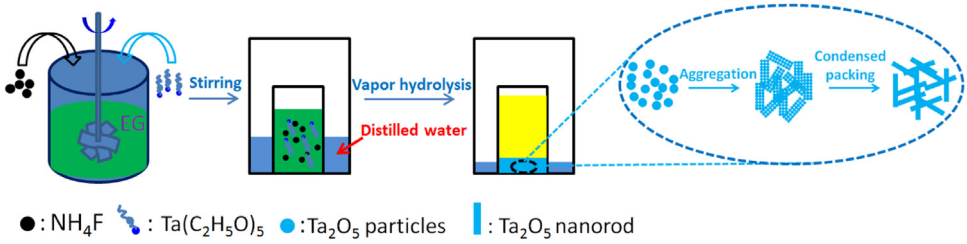

Scheme 1. The schematic illustration of the formation procedure of the crystallized self-doped Ta_2O_5 nanorod.

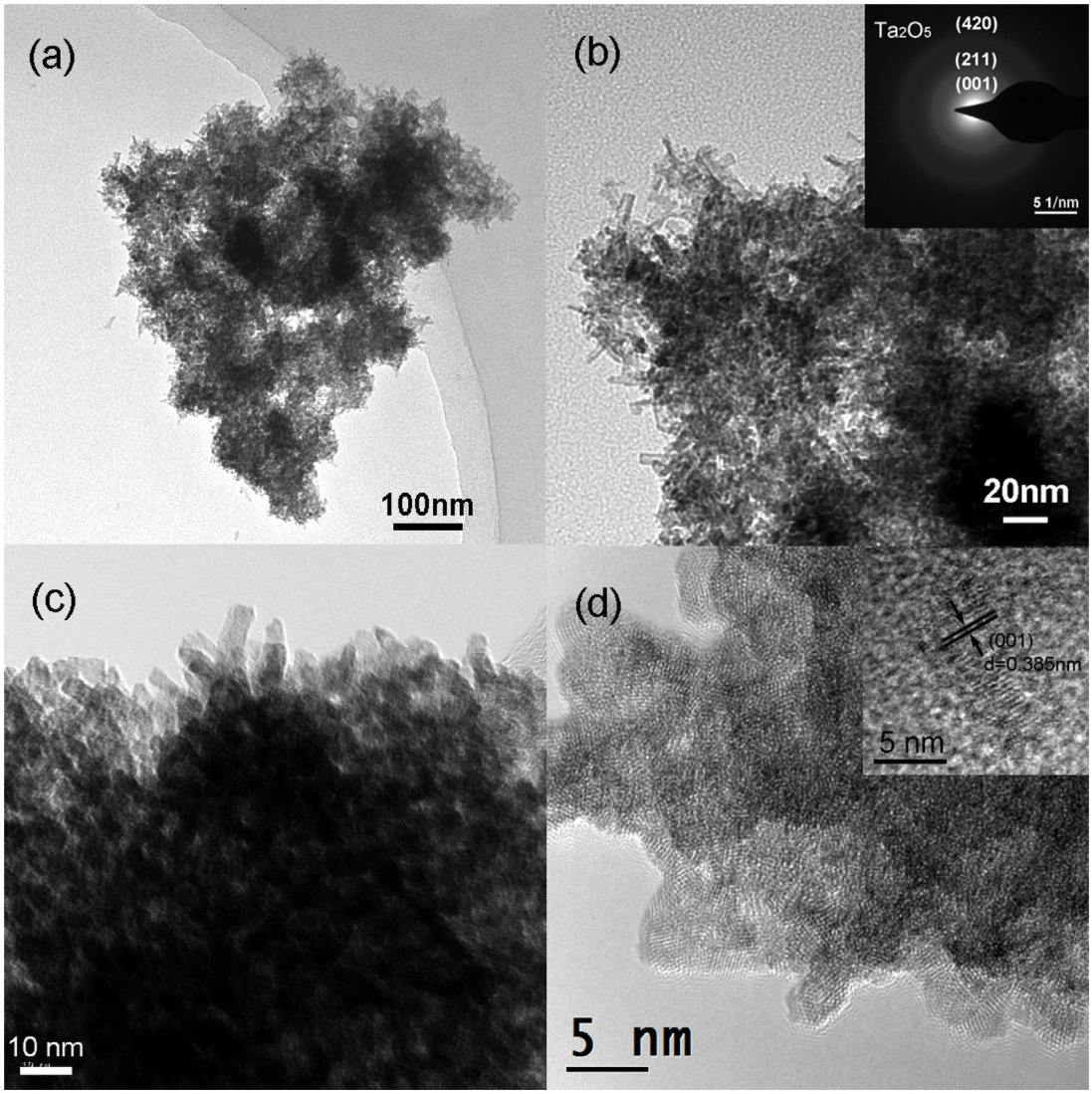

Fig. 1. Typical TEM images (a; b, SAED pattern (insert); c), HRTEM image (d) of the self-doped Ta_2O_5-220 nanorod.

220 catalyst was composed of many Ta_2O_5 nanorod and had a slight agglomeration in spite of the existence of ethylene glycol. Fig. 1(b) displayed the magnified image of Ta_2O_5 nanorod, which clearly displayed the morphology of Ta_2O_5 nanorod. The insert in Fig. 1(b) was the selected area electron diffraction (SAED) pattern, which further confirmed the polycrystalline nature of the as-prepared Ta_2O_5 nanorod. Fig. 1(c) further clearly displayed the morphology of Ta_2O_5 nanorod. Fig. 1(d) clearly displayed the HRTEM image of the self-doped Ta_2O_5 nanorod with a plane spacing of 0.385 nm (insert), which corresponded to the d spacing of Ta_2O_5 (001) plane, and the self-doped Ta_2O_5 nanorod was about 5 nm in diameter and 15 nm in length according to HRTEM image (Fig. 1(d)), further confirming the formation of Ta_2O_5 nanorod.

Fig. 2 displayed the XRD patterns of the self-doped Ta_2O_5 nanorod prepared at different hydrolysis temperatures. The XRD patterns of the self-doped Ta_2O_5 nanorod well agreed with the standard card of JCPDS No.08-0255 ($a = 6.180$, $b = 3.660$, $c = 3.880$, $\alpha = \beta = \gamma = 90.00^\circ$). The typical diffraction peaks at 22.96°, 28.31°, 28.87°, 36.96°, 46.53°, 55.26°, 70.30° and 79.87° respectively corresponded to (001), (110), (200), (201), (002), (021), (411) and (130) planes of Ta_2O_5, which indicated the pure Ta_2O_5 was successfully fabricated by vapor hydrolysis treatment yet not other chemicals, such as H_2TaO_6, or $Ta_2O_5{\cdot}nH_2O$ [40]. That is, F element produced

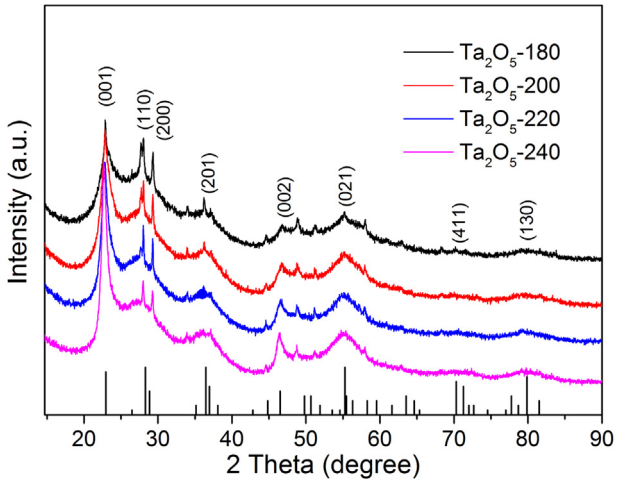

Fig. 2. XRD patterns of the self-doped Ta_2O_5 nanorod.

from the decomposition of NH_4F in this experiment was not doped into lattice of the as-prepared Ta_2O_5 nanorod, and just adsorbed on the surface of the self-doped Ta_2O_5 nanorod. Besides, the intensity of the diffraction peak of the self-doped Ta_2O_5 nanorod became stronger with the increase of the reaction temperatures, indicating a higher crystallinity at a higher hydrolysis temperature, in which NH_4F could be decomposed into HF and NH_3 in the vapor hydrolysis process, and HF formed a weak acidic condition for the amorphous phase dissolution and crystalline phase formation [36,41].

Fig. 3 displayed the XPS spectra (a, b and c) of the commercial Ta_2O_5 and the as-prepared self-doped Ta_2O_5 nanorod, high-angle annular dark-field scanning transmission electron microscope (HAADF-STEM) image and the corresponding EDS mappings (d) of the self-doped Ta_2O_5 nanorod. As shown in Fig. 3(a), the Ta 4f XPS spectra confirmed the presence of Ta^{4+} species in the self-doped Ta_2O_5 nanorod. The binding energy of $Ta4f_{5/2}$ and $Ta4f_{7/2}$ for commercial Ta_2O_5 were 28.26 and 26.37 eV, but the binding energy of $Ta4f_{5/2}$ and $Ta4f_{7/2}$ for the self-doped Ta_2O_5 nanorod was 27.92 and 26.01 eV, respectively. That was, the $Ta4f_{5/2}$ and $Ta4f_{7/2}$ peaks of the self-doped Ta_2O_5 nanorod shifted from higher binding energy to a lower binding energy in comparison to those of commercial Ta_2O_5, which was very familiar to the binding energy shift of Ti^{3+} species in TiO_2 in the literatures [42–44], further demonstrating the formation of Ta^{4+} species in the self-doped Ta_2O_5 nanorod [43]. Fig. 3(b) showed the O1s spectra of commercial Ta_2O_5 and the self-doped Ta_2O_5 nanorod. The O1s spectra of the commercial Ta_2O_5 could be fitted into two peaks centered at 530.10 and 531.66 eV, which was ascribed to Ta-O bond and surface −OH groups [45], respectively. And the O1s spectra of the self-doped Ta_2O_5 could be also fitted into two peaks at 529.08 and 530.29 eV, which could be ascribed to surface −OH groups, oxygen vacancy neighbors to Ta^{4+} species and the lattice oxygen atoms of Ta_2O_5 [43,46,47]. And Ta^{4+} species generated with the generation of oxygen vacancy during the vapor hydrolysis process [43], which also further confirmed the formation of Ta^{4+} species in the self-doped Ta_2O_5 nanorod, and was consistent with the result of XPS valence band spectra of the as-prepared Ta_2O_5 nanorod in Fig. S1. The Fig. 3(c) showed the F1s spectra of the as-prepared Ta_2O_5 nanorod. The peak at 683.16 eV should be assigned to the typical surface fluorid, which was very similar to F^- species in Ta_2O_5 or TiO_2 reported in literatures [36,48]. It was reported that the binding energy of the lattice F was about 688.5–689.6 eV [48,49], much higher than that of F (683.16 eV) absorbed on the surface of the Ta_2O_5 nanorod, which indicated that fluorine ions of the self-doped Ta_2O_5 in this experiment were the typical surface fluorine species and only adsorbed on the surface yet not incorporated into Ta_2O_5 lattice to substitute oxygen ions. And the surface fluorine in this experiment contributed to promote the crystallization of Ta_2O_5 nanorod, which was very similar to some previous reports [36,38,43], and good consistent with the HRTEM (Fig. 1(d)) and XRD (Fig. 2) results. The HAADF-STEM image in Fig. 3(d) also further revealed the Ta_2O_5 nanorod morphology, which was good consistent with the HRTEM results in Fig. 1(d). And Fig. 3(d) also displayed the corresponding EDS mapping of the self-doped Ta_2O_5 nanorod, which indicated the self-doped Ta_2O_5 nanorod was consist of Ta, O and F elements. Above all, we could conclude that the crystallized self-doped Ta_2O_5 nanorod was successfully prepared.

Fig. 4 showed the colors (inserts of Fig. 4(a)) and UV–vis diffuse reflectance absorption spectra of the commercial Ta_2O_5 and self-doped Ta_2O_5 nanorod. The colors of the self-doped Ta_2O_5 regularly turned dark brown from light grey with the increase of the vapor hydrolysis temperatures, indicating the stronger visible light harvesting capacity [50,51], while the color of commercial Ta_2O_5 was nearly white. As shown in Fig. 4 (a), the commercial Ta_2O_5 catalyst displayed strong UV light absorption with an absorption edge of ~320 nm yet no visible light absorption, which was consistent with reported literatures [52–54], but the self-doped Ta_2O_5 nanorod showed strong visible light absorption in the range of 400–800 nm, which indicated the self-doped Ta_2O_5 nanorod had strong visible-light harvesting capacity for photocatalytic hydrogen production, which was well consistent with the color changes of the self-doped Ta_2O_5 nanorod. The spectral absorption edges of the self-doped Ta_2O_5 had a red shift with the increase of the hydrolysis temperatures, which indicated the hydrolysis temperatures could alter the band gaps of the self-doped Ta_2O_5 nanorod. That is, the excellent visible light absorption of the self-doped Ta_2O_5 was attributed to the formation of new defect energy level composed by Ta^{4+} species. And the estimated optical band gaps of commercial Ta_2O_5 and the self-doped Ta_2O_5 nanorod were displayed in Fig. 4(b) according the Tauc equation,

$$Ah\nu = (\alpha h\nu\text{-}Eg)^{1/2} \quad (1)$$

where A is the absorbance, h is Planck's constant, ν is photon frequency, α is the absorption coefficient, Eg is the estimated band gap of the semiconductor. The estimated band gaps of the commercial Ta_2O_5, Ta_2O_5-180, Ta_2O_5-200, Ta_2O_5-220 and Ta_2O_5-240 were about 3.83, 2.93, 2.83, 2.75 and 2.53 eV, respectively [55,56], which indicated the higher hydrolysis temperatures were beneficial to generate more Ta^{4+} species in the self-doped Ta_2O_5 nanorod to effectively narrow the band gap of the as-prepared Ta_2O_5 nanorod [50].

Fig. 5 showed the Nitrogen adsorption-desorption isotherm and the specific surface areas (insert) of the self-doped Ta_2O_5 nanorod. As shown in Fig. 5, Ta_2O_5-180, Ta_2O_5-200, Ta_2O_5-220 and Ta_2O_5-240 catalysts presented the type IV isotherms with H2 hysteresis loop, which were the typical characteristics of mesoporous Ta_2O_5 catalysts. And the mesopores were formed by the aggregation of Ta_2O_5 nanorod, and favour of harvesting visible light and the generated hydrogen diffusion from the reaction active sites to the methanol aqueous solution. The specific surface areas of Ta_2O_5-180, Ta_2O_5-200, Ta_2O_5-220 and Ta_2O_5-240 catalysts were up to 207.633, 237.887, 200.739 and 204.342 m^2/g, as shown in Fig. 5 (inset), which were much higher than those of commercial Ta_2O_5 and some reported Ta_2O_5 catalysts in the literatures [35,56–61]. And the high specific surface areas could offer more active sites for hydrogen production. As we all know, the crystallization and specific surface areas both have great influences on the photocatalytic activity of the photocatalysts [62]. In general, the increase of the crystallization often decreased the specific surface areas, which might be detrimental for the enhancement of the photocatalytic activity. However, the specific surface areas of the self-doped

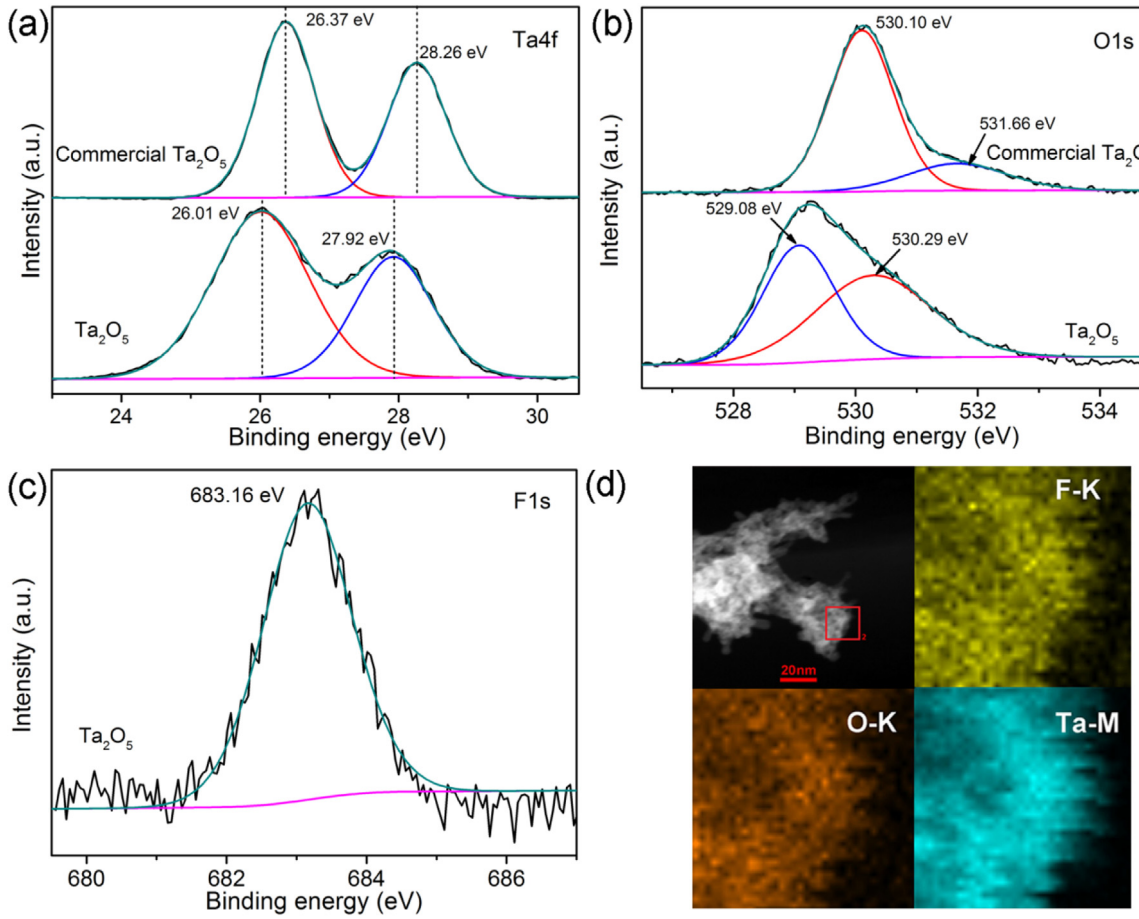

Fig. 3. XPS spectra of commercial Ta_2O_5 and the self-doped Ta_2O_5-220 nanorod: (a) Ta 4f, (b) O 1s, (c) F1s and (d) HAADF-STEM image and the corresponding EDS mapping of the self-doped Ta_2O_5-220 nanorod.

Ta_2O_5 nanorod in this experiment could reach up to 237.887 m^2/g, though the crystallization of the self-doped Ta_2O_5 nanorod was highly promoted by fluorine ions, which showed great advantages of the vapor hydrolysis with NH_4F as morphology regulating agent.

EPR spectra of commercial Ta_2O_5 and the self-doped Ta_2O_5 nanorod were measured to investigate the Ta^{4+} species neighbors to oxygen vacancy defect of the self-doped Ta_2O_5 nanorod. As shown in Fig. 6, the commercial Ta_2O_5 showed no detectable EPR signal, indicating no Ta^{4+} species or oxygen vacancy defect existing in the commercial Ta_2O_5. And therefore, the commercial Ta_2O_5 did not response to visible light because of its typical wide band gap (~3.83 eV). However, the self-doped Ta_2O_5 catalysts in this experiment displayed strong EPR signals around at g = 2.086, which indicated oxygen vacancy defects were indeed generated. As we know, oxygen vacancy defect was formed along with the generation of Ta^{4+} species [43,63]. That is, only the Ta^{4+} species was generated but not other defects according to the charge-neutrality principle and energy state relationships, which was responsible for the visible-light absorption and visible-light photocatalytic activity of the self-doped Ta_2O_5 nanorod for hydrogen production. Besides, the EPR signals of all the self-doped Ta_2O_5 catalysts in this experiment displayed strong EPR signals around at g = 2.086, which indicated oxygen vacancy defects were generated. And the EPR signals of the as-prepared self-doped Ta_2O_5 nanorod increased progressively in intensity with the increase of the hydrolysis temperatures in this experiment, which indicated that Ta^{4+} species seemed to be controlled and regulated by adjusting the vapor hydrolysis temperatures. In general, the Ta^{4+} species (oxygen vacancy defects) in the self-doped Ta_2O_5 nanorod could also be as the recombination centers of the photo-induced electrons and holes, and an excess of the Ta^{4+} species or oxygen vacancy was adverse to enhance the photocatalytic activity of the Ta_2O_5 nanorod for hydrogen production [43]. However, the content of the generated Ta^{4+} species in this experiment seemed to be rather limited and availed for the photocatalytic activity of the self-doped Ta_2O_5 nanorod for hydrogen production yet not as the recombination centers of photo-induced electron-hole pairs. The new formed Ta^{4+} species efficiently harvested the visible light and promoted the separation of the photo-induced electron-hole pairs [50,64]. Based on this, it could be concluded that the hydrolysis temperatures in this experiment greatly influenced the formation of Ta^{4+} species in the self-doped Ta_2O_5 nanorod.

Surface photovoltage spectroscopy, an effective tool to investigate the amount of charge (Q) spatial separation [65,66], is the photovoltaic effects of solid surface. As displayed in Fig. 7(a), the as-prepared self-doped Ta_2O_5 nanorod showed strong positive surface photovoltage response in the range of ~300–420 nm, a typical characteristic of n-type semiconductors [67], which indicated the recombination of the photo-induced electron-hole pairs were highly suppressed and had a good charge separating efficiency. Besides, the surface photovoltage reponse of Ta_2O_5-220 was strongest than the other three samples, indicating the excellent charge separating efficiency, which was also consistent with the trend of the photocatalytic performances below, much like the reported CdS/ZnO heterostructure [68]. Fig. 7(b) showed the surface photovoltage response of Ta_2O_5-220 catalysts with different electrical fields. The surface photovoltage response increased rapidly with the increase of the external positive bias potential,

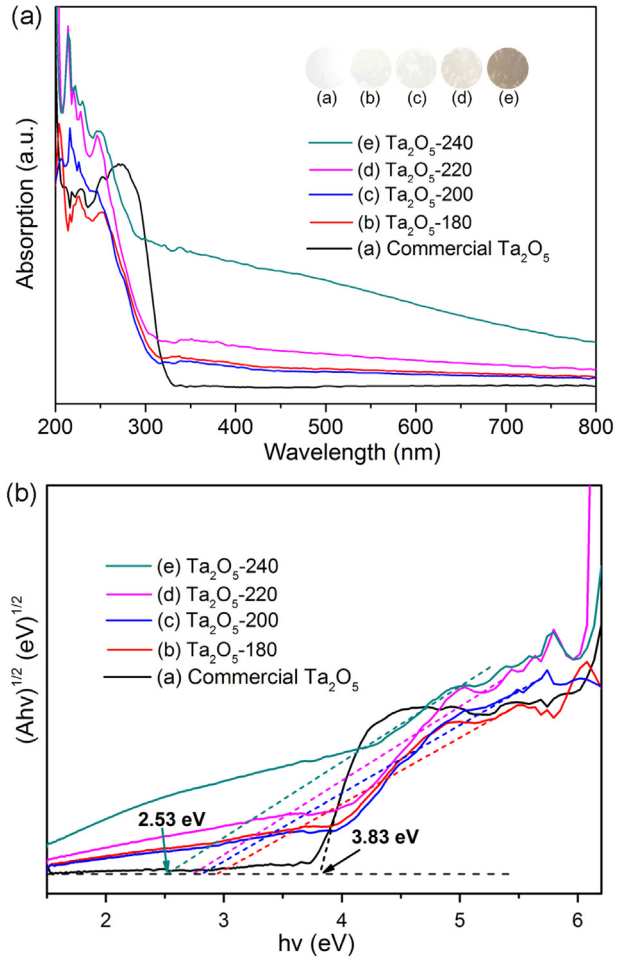

Fig. 4. (a) UV–vis diffuse reflectance absorption spectra and (b) estimated band gaps of the commercial Ta_2O_5 and the self-doped Ta_2O_5 nanorod.

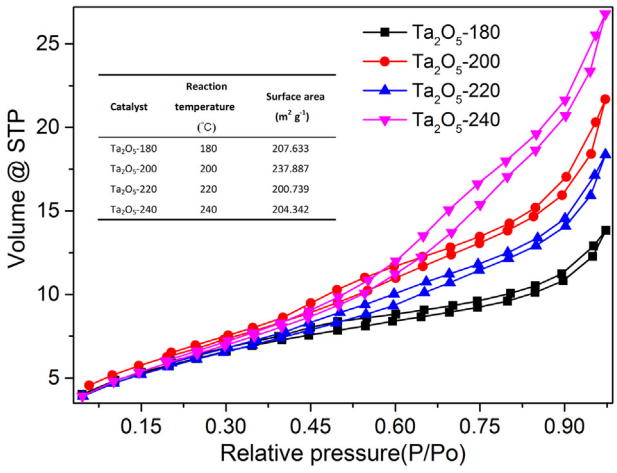

Fig. 5. Nitrogen adsorption-desorption isotherm (inset: the surface area) of the self-doped Ta_2O_5 nanorod.

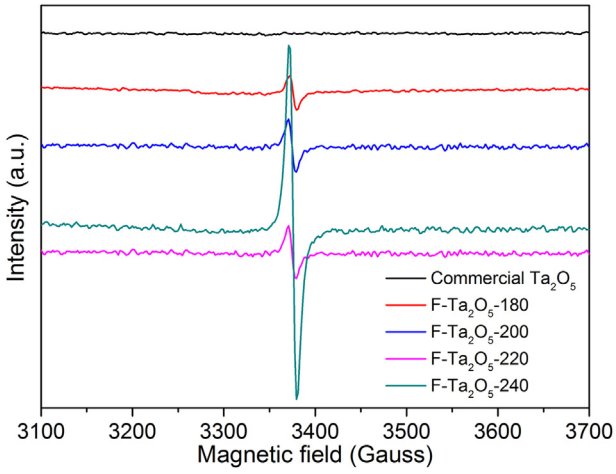

Fig. 6. EPR spectra of the commercial Ta_2O_5 and the self-doped Ta_2O_5 nanorod.

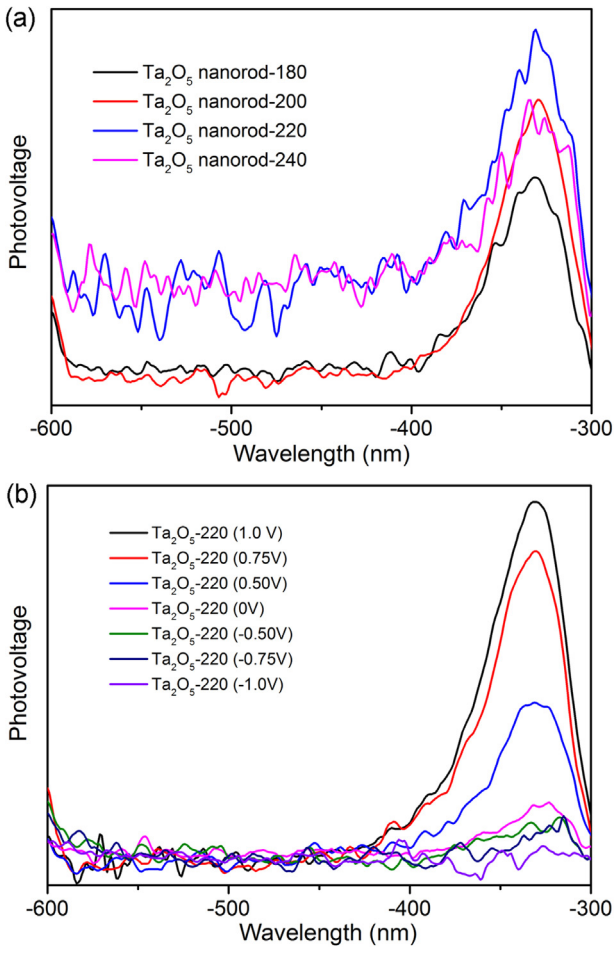

Fig. 7. (a) SPV spectra of the self-doped Ta_2O_5 nanorod and (b) surface photovoltage response of Ta_2O_5-220 catalysts with different electrical fields.

indicating the direction of internal built electric field of the self-doped Ta_2O_5 was in accordance with that of the external positive field. The positive field was favour for the charge carrier separation of the as-prepared self-doped Ta_2O_5 nanorod. However, the surface photovoltage response decreased regularly with the external negative bias potential, indicating the external negative field was against the internal built electric field of the self-doped Ta_2O_5 nanorod, and this phenomenon was much like that of the flower-like ZnO nanostructures [69]. And therefore, the visible light response range could be extended by adjusting the external positive bias voltage [70], which indicated the self-doped Ta_2O_5 nanorod perhaps an excellent photoelectric functional material [69].

Electrochemical impendence spectra (EIS) were used to investigate the charge transfer resistance to confirm the important roles of Ta^{4+} species in the self-doped Ta_2O_5 nanorod with a

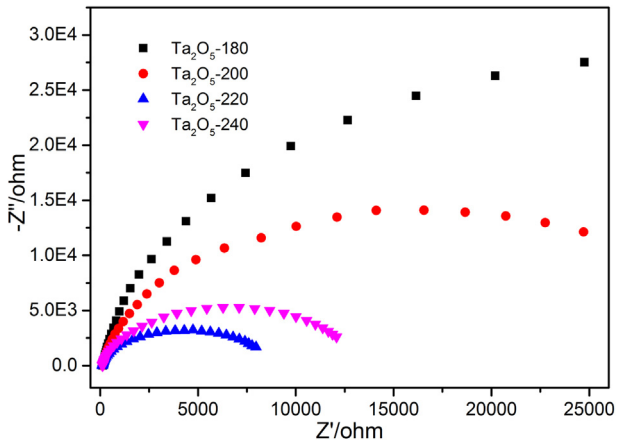

Fig. 8. EIS spectra of the commercial Ta_2O_5 and the self-doped Ta_2O_5 nanorod.

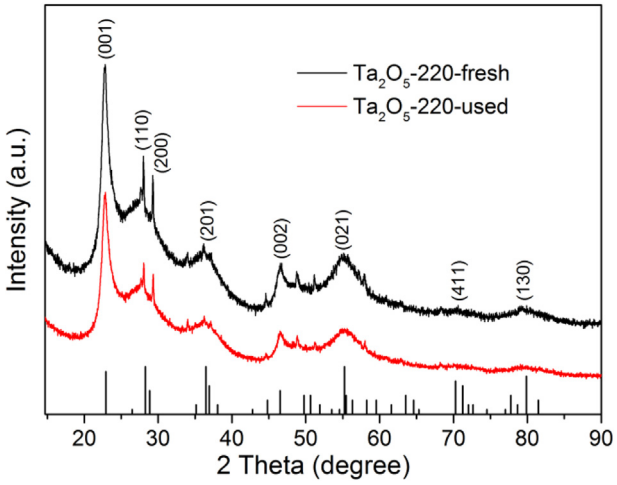

Fig. 9. XRD patterns of the fresh and the used self-doped Ta_2O_5 nanorod.

three-electrode cell, as displayed in Fig. 8. The Ta_2O_5-180 catalyst presented the largest arc radiuses in comparison to the other three samples, which indicated the strongest charge transfer resistance. And the Ta_2O_5-220 nanorod displayed the smallest the arc radiuses, which indicated the Ta_2O_5-220 nanorod had the smallest charge transfer resistance and highest separation efficiency of the photo-induced electrons and holes, and these results were consistent with the following photocatalytic H_2 production activity, further confirming the important roles of Ta^{4+} species in the self-doped Ta_2O_5 nanorod.

The XRD patterns of the fresh Ta_2O_5-220 nanorod and the used Ta_2O_5-220 nanorod were used to investigate the chemical stability of the self-doped Ta_2O_5 nanorod, as displayed in Fig. 9. The XRD patterns of the used Ta_2O_5-220 nanorod seemed like the same to that of the fresh Ta_2O_5-220 nanorod with just a slightly decrease in intensity like g-C_3N_4 isotype composite [71–73], which further confirmed the stability of the chemical structure of the self-doped Ta_2O_5-220 nanorod.

Fig. 10 showed the photocatalytic hydrogen evolution activity of the commercial Ta_2O_5 and the self-doped Ta_2O_5 nanorod under UV light, simulated sunlight and visible light irradiation. As shown in Fig. 10(a), the self-doped Ta_2O_5 nanorod displayed highly enhanced photocatalytic activity for hydrogen production in comparison to that of the commercial Ta_2O_5 under UV light irradiation, and the photocatalytic activity of the self-doped Ta_2O_5 nanorod could reach up to 10.17×10^3 μmol g^{-1} h^{-1}, mainly because of the enhanced charge separation efficiency induced by Ta^{4+} species in the self-doped Ta_2O_5 nanorod. Besides, the highest specific surface area of self-doped Ta_2O_5 nanorod in this experiment (237.887 m^2/g) was 103.43-fold than that of the commercial Ta_2O_5 (2.3 m^2/g) [37], which could offer more active sites for photocatalytic hydrogen production. The photocatalytic activity of the self-doped Ta_2O_5 nanorod under simulated sunlight irradiation was also highly enhanced in comparison to that of commercial

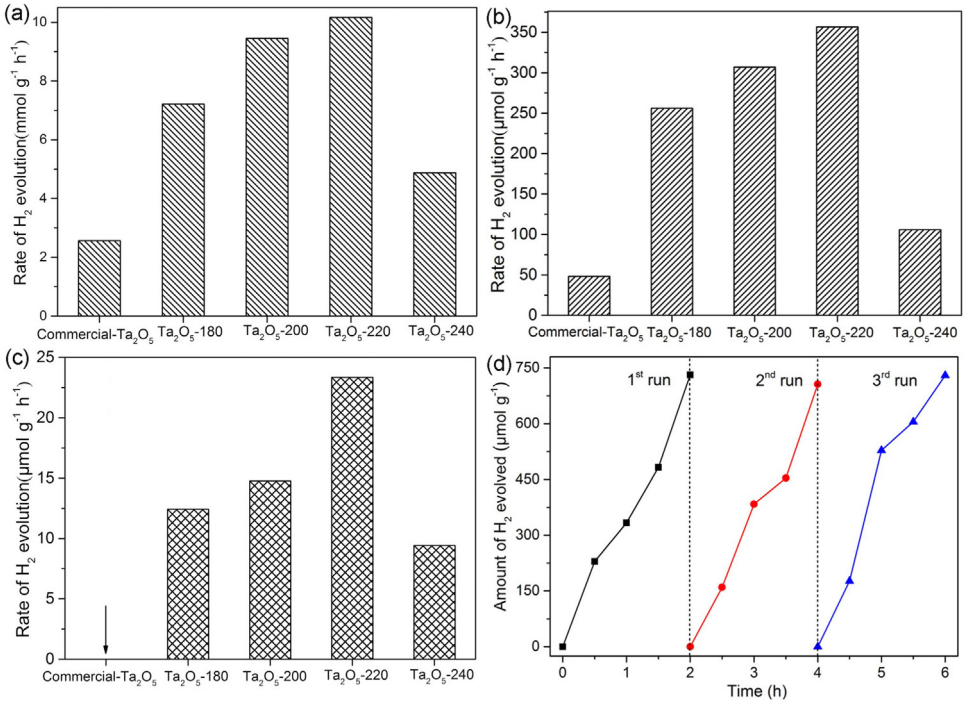

Fig. 10. The photocatalytic hydrogen evolution rate of the commercial Ta_2O_5 and the self-doped Ta_2O_5 nanorod (a) UV light (λ > 200 nm); (b) simulated sunlight (λ > 320 nm); (c) visible light (λ > 400 nm) and (d) the recyclable photocatalytic activity of Ta_2O_5-220 catalyst under simulated sunlight irradiation.

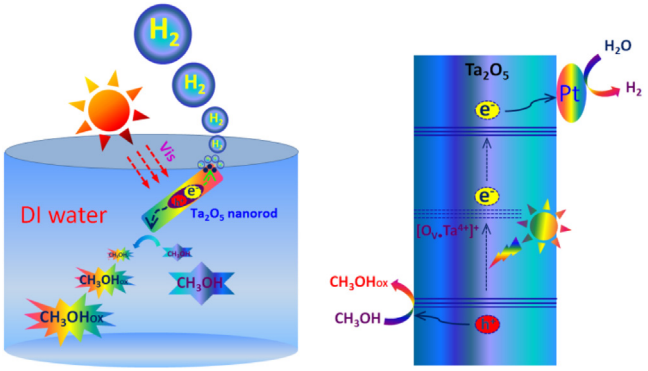

Fig. 11. Proposed visible light photocatalysis mechanisms of the self-doped Ta_2O_5 nanorod for hydrogen production.

Ta_2O_5, which could reach up to 356.68 μmol g^{-1} h^{-1} (Fig. 10(b)). To the best of my knowledge, the visible light photocatalytic activity of Ta_2O_5 catalysts without noble metals (eg. Au, Ag and Cu) for hydrogen production is still a great challenge and hot focus nowadays [74,75]. As we all know, the commercial Ta_2O_5 had no visible light absorption and visible light photocatalytic activity for hydrogen production. However, the self-doped Ta_2O_5 nanorod in this experiment displayed amazing visible light absorption and visible light photocatalytic activity for hydrogen production. As seen in Fig. 10(c), the visible light photocatalytic activity of the self-doped Ta_2O_5 nanorod could reach up to 23.35 μmol g^{-1} h^{-1}, showing great advantage in comparison to that of the commercial Ta_2O_5, which was attributed to the formation of the defect energy level composed of Ta^{4+} species in the self-doped Ta_2O_5 nanorod, and consistent with the results in Fig. S2. Of course, the high specific surface area, mesoporous structure, and relatively high crystallinity of the self-doped Ta_2O_5 nanorod were also favour of the photocatalytic hydrogen production under visible light irradiation. Fig. 10(d) displayed the recyclable photocatalytic activity of the self-doped Ta_2O_5-220 catalyst under simulated sunlight irradiation, further confirming good photocatalytic stability under the simulated sunlight irradiation.

We also investigated the visible light photocatalytic mechanism of the self-doped Ta_2O_5 nanorod for hydrogen production in detail, as shown in Fig. 11. The valence band and conduction band of the commercial Ta_2O_5 semiconductor were reported to be about −0.17 and +3.83 eV [30,76]. And therefore, the commercial Ta_2O_5 showed no visible light response because of its typical wide band gap (~4.0 eV). Nevertheless, the wide band gap of Ta_2O_5 could provide a strong driving force for hydrogen production in thermodynamics, suggesting the wide band gap Ta_2O_5 semiconductor a promising and potential photocatalyst for hydrogen production. In this experiment, the Ta^{4+} species neighbors to oxygen vacancy defects in the self-doped Ta_2O_5 nanorod was generated by vapor hydrolysis treatment with ethylene glycol as reductant and stabilizer, which formed a new defect energy level between the valence band maximum and conduction band minimum of the self-doped Ta_2O_5 nanorod, and effectively narrowed the band gap of the as-prepared Ta_2O_5 nanorod [77–79], making the Ta_2O_5 nanorod effectively capture the visible light. And thus, the photo-induced electrons from the valence band of the self-doped Ta_2O_5 under visible light irradiation would leaped into the new formed defect energy level and then transferred to the conduction band of the self-doped Ta_2O_5 for hydrogen production at active sites of noble metal, and the generated holes was removed by methanol [80,81]. The Ta^{4+} species in this experiment was beneficial for charge separation yet not the recombination centers of photo-induced electron-hole pairs, which indicated that the vapor hydrolysis was more suitable for preparing defect-rich semiconductor with ethylene glycol as mild reductant. It was the formation of the defect energy level composed by Ta^{4+} species between the valence band maximum and conduction band minimum that the self-doped Ta_2O_5 nanorod displayed inspiring visible light photocatalytic activity for hydrogen production.

4. Conclusions

We successfully synthesized a novel Ta^{4+} self-doped Ta_2O_5 nanorod by facile vapor hydrolysis method. The hydrolysis temperatures played an important role in the formation of Ta^{4+} species in the NH_4F-ethylene glycol mixture, and the fluorine ions, produced from the decomposition of NH_4F, highly promoted the crystallization of Ta_2O_5 nanorod in the weak acid environment, which contributed to suppress the recombination of the photo-induced electron-hole pairs, confirmed by SPV technology. The self-doped Ta_2O_5 nanorod displayed highly enhanced UV light, simulated sunlight and visible light photocatalytic activity for hydrogen production as well as the amazing visible light absorption from 400 to 800 nm, mainly because of the formation of Ta^{4+} species, high specific surface area, mesoporous structure and promoted crystallization of the self-doped Ta_2O_5 nanorod, which showing its great advantages in comparison to those of commercial Ta_2O_5. Besides, this experiment might also offer a new method to prepare the defect-rich metal-oxide semiconductors in the mild reaction environment for visible light photocatalysis.

Acknowledgments

The authors would like to thank the partial financial support from the National Natural Science Foundation of China under grant no.51272052 and 50902040, the Heilongjiang Province Science Foundation for Young Scholar (QC2010065).

References

[1] A. Kudo, Y. Miseki, Chem. Soc. Rev. 38 (2009) 253–278.
[2] H. Tong, S. Ouyang, Y. Bi, N. Umezawa, M. Oshikiri, J. Ye, Adv. Mater. 24 (2012) 229–251.
[3] P. Zhang, J. Zhang, J. Gong, Chem. Soc. Rev. 43 (2014) 4395–4422.
[4] J. Yang, D. Chen, Y. Zhu, Y. Zhang, Y. Zhu, Appl. Catal. B-Environ. 205 (2017) 228–237.
[5] X. Bai, C. Sun, D. Liu, X. Luo, D. Li, J. Wang, N. Wang, X. Chang, R. Zong, Y. Zhu, Appl. Catal. B-Environ. 204 (2017) 11–20.
[6] A. Fujishima, K. Honda, Nature 238 (1972) 37–38.
[7] J. Willkomm, K.L. Orchard, A. Reynal, E. Pastor, J.R. Durrant, E. Reisner, Chem. Soc. Rev. 45 (2015) 9–23.
[8] X. Li, J. Yu, M. Jaroniec, Chem. Soc. Rev. 45 (2016) 2603–2636.
[9] M. Tahir, N.S. Amin, Energy Convers. Manage. 76 (2013) 194–214.
[10] W. Zhou, H. Fu, Chemcatchem 5 (2013) 885–894.
[11] H. Xu, S. Ouyang, L. Liu, P. Reunchan, N. Umezawa, J. Ye, J. Mater. Chem. A 2 (2014) 12642–12661.
[12] G. Zhu, T. Lin, H. Cui, W. Zhao, H. Zhang, F. Huang, Acs Appl. Mater. Inter. 8 (2016) 122–127.
[13] J. Qi, K. Zhao, G. Li, Y. Gao, H. Zhao, R. Yu, Z. Tang, Nanoscale 6 (2014) 4072–4077.
[14] A. Tanaka, K. Hashimoto, H. Kominami, J. Am. Chem. Soc. 134 (2012) 14526–14533.
[15] X. Chen, S. Shen, L. Guo, S.S. Mao, Chem. Rev. 110 (2010) 6503–6570.
[16] A.A. Ismail, D.W. Bahnemann, Sol. Energy Mater. Sol. Cells 128 (2014) 85–101.
[17] A.J. Esswein, D.G. Nocera, Chem. Rev. 107 (2007) 4022–4047.
[18] X. Wang, K. Maeda, X. Chen, K. Takanabe, K. Domen, Y. Hou, X. Fu, M. Antonietti, J. Am. Chem. Soc. 131 (2009) 1680–1681.
[19] J. Schneider, M. Matsuoka, M. Takeuchi, J. Zhang, Y. Horiuchi, M. Anpo, D.W. Bahnemann, Chem. Rev. 114 (2014) 9919–9986.
[20] W. Hou, S.B. Cronin, Adv. Funct. Mater. 23 (2013) 1612–1619.
[21] H. Li, Z. Bian, J. Zhu, Y. Huo, H. Li, Y. Lu, J. Am. Chem. Soc. 129 (2007) 4538–4539.
[22] A. Iwase, H. Kato, A. Kudo, Appl. Catal. B-Environ. 136 (2013) 89–93.
[23] X. Zhang, T. Peng, S. Song, J. Mater. Chem. A 4 (2016) 2365–2402.
[24] X. Wang, G. Sun, N. Li, P. Chen, Chem. Soc. Rev. 45 (2016) 2239–2262.
[25] S. Wang, L. Pan, J.J. Song, W. Mi, J.J. Zou, L. Wang, X. Zhang, J. Am. Chem. Soc. 137 (2015) 2975–2983.
[26] H. Yu, Y. Zhao, C. Zhou, L. Shang, Y. Peng, Y. Cao, L.-Z. Wu, C.-H. Tung, T. Zhang, J. Mater, Chem. A 2 (2014) 3344–3351.

[27] Y.H. Lv, Y.Y. Zhu, Y.F. Zhu, J. Phys. Chem. C 117 (2013) 18520–18528.
[28] W.J. Chun, A. Ishikawa, H. Fujisawa, T. Takata, J.N. Kondo, M. Hara, M. Kawai, Y. Matsumoto, K. Domen, J. Phys. Chem. B 107 (2003) 1798–1803.
[29] S. Anandan, N. Pugazhenthiran, T. Selvamani, S.-H. Hsieh, G.-J. Lee, J.J. Wu, Catal. Sci. Technol. 2 (2012) 2502–2507.
[30] Y. Luo, X. Liu, X. Tang, Y. Luo, Q. Zeng, X. Deng, S. Ding, Y. Sun, J. Mater. Chem. A 2 (2014) 14927–14939.
[31] X. Wang, K. Maeda, A. Thomas, K. Takanabe, G. Xin, J.M. Carlsson, K. Domen, M. Antonietti, Nature Mater. 8 (2009) 76–80.
[32] F.E. Osterloh, Chem. Soc. Rev. 42 (2013) 2294–2320.
[33] P. Zhou, J. Yu, M. Jaroniec, Adv. Mater. 26 (2014) 4920–4935.
[34] C. Tao, L. Xu, J. Guan, Chem. Eng. J. 229 (2013) 371–377.
[35] R.V. Goncalves, P. Migowski, H. Wender, D. Eberhardt, D.E. Weibel, F.C. Sonaglio, M.J.M. Zapata, J. Dupont, A.F. Feil, S.R. Teixeira, J. Phys. Chem. C 116 (2012) 14022–14030.
[36] Z. Li, J. Liu, J. Li, J. Shen, Nanoscale 4 (2012) 3867–3870.
[37] L. Guo, H. Hagiwara, S. Ida, T. Daio, T. Ishihara, Acs Appl. Mater. Inter. 5 (2013) 11080–11086.
[38] J. Duan, W. Shi, L. Xu, G. Mou, Q. Xin, J. Guan, Chem. Commun. 48 (2012) 7301–7303.
[39] J. Liu, S. Wen, Y. Hou, F. Zuo, G.J.O. Beran, P. Feng, Angew. Chem. Int. Ed. 52 (2013) 3241–3245.
[40] X. Yu, Y. Wei, Z. Li, J. Liu, Mater. Lett. 191 (2017) 150–153.
[41] J. Yu, J. Zhang, Dalton Trans. 39 (2010) 5860–5867.
[42] J. Huo, Y. Hu, H. Jiang, C. Li, Nanoscale 6 (2014) 9078–9084.
[43] M. Xing, W. Fang, M. Nasir, Y. Ma, J. Zhang, M. Anpo, J. Catal. 297 (2013) 236–243.
[44] W. Liao, M. Murugananthan, Y. Zhang, Phys. Chem. Chem. Phys. 17 (2015) 8877–8884.
[45] K. Li, S. Gao, Q. Wang, H. Xu, Z. Wang, B. Huang, Y. Dai, J. Lu, Acs Appl. Mater. Inter. 7 (2015) 9023–9030.
[46] W. Fang, M. Xing, J. Zhang, Appl. Catal. B-Environ. 160 (2014) 240–246.
[47] X. Yu, Z. Li, J. Liu, P. Hu, Appl. Catal. B-Environ. 205 (2017) 271–280.
[48] Q. Zhang, R. Li, Z. Li, A. Li, S. Wang, Z. Liang, S. Liao, C. Li, J. Catal. 337 (2016) 36–44.
[49] H. Park, W. Choi, J. Phys. Chem. B 108 (2004) 4086–4093.
[50] Y. Zhou, C. Chen, N. Wang, Y. Li, H. Ding, J. Phys. Chem. C 120 (2016) 6116–6124.
[51] Y.H. Lv, C.S. Pan, X.G. Ma, R.L. Zong, X.J. Bai, Y.F. Zhu, Appl. Catal. B-Environ. 138 (2013) 26–32.
[52] L. Xu, X. Sun, H. Tu, Q. Jia, H. Gong, J. Guan, Appl. Catal. B-Environ. 184 (2016) 309–319.
[53] H. Sakamoto, T. Ohara, N. Yasumoto, Y. Shiraishi, S. Ichikawa, S. Tanaka, T. Hirai, J. Am. Chem. Soc. 137 (2015) 9324–9332.
[54] J. Li, W. Dai, G. Wu, N. Guan, L. Li, Catal. Commun. 65 (2015) 24–29.
[55] K. Li, A.D. Handoko, M. Khraisheh, J. Tang, Nanoscale 6 (2014) 9767–9773.
[56] A.A. Ismail, M. Faisal, F.A. Harraz, A. Al-Hajry, A.G. Al-Sehemi, J. Colloid Interface Sci. 471 (2016) 145–154.
[57] R.V. Goncalves, R. Wojcieszak, P.M. Uberman, D. Eberhardt, E. Teixeira-Neto, S.R. Teixeira, L.M. Rossi, Catal. Commun. 48 (2014) 50–54.
[58] X. Lu, S. Ding, T. Lin, X. Mou, Z. Hong, F. Huang, Dalton Trans. 41 (2012) 622–627.
[59] T. Sreethawong, S. Ngamsinlapasathian, Y. Suzuki, S. Yoshikawa, J. Mol. Catal. A: Chem. 235 (2005) 1–11.
[60] T. Sreethawong, S. Ngamsinlapasathian, S. Yoshikawa, J. Mol. Catal. A: Chem. 374 (2013) 94–101.
[61] R.V. Gonçalves, P. Migowski, H. Wender, D. Eberhardt, D.E. Weibel, F.C. Sonaglio, M.J.M. Zapata, J. Dupont, A.F. Feil, S.R. Teixeira, J. Phys. Chem. C 116 (2012) 14022–14030.
[62] L. Xu, J. Guan, W. Shi, L. Liu, J. Colloid Interface Sci. 377 (2012) 160–168.
[63] Y.H. Lv, Y.F. Liu, Y.Y. Zhu, Y.F. Zhu, J. Mater. Chem. A 2 (2014) 1174–1182.
[64] X.J. Bai, L. Wang, R.L. Zong, Y.H. Lv, Y.Q. Sun, Y.F. Zhu, Langmuir 29 (2013) 3097–3105.
[65] T. Jiang, T. Xie, W. Yang, L. Chen, H. Fan, D. Wang, J. Phys. Chem. C 117 (2013) 4619–4624.
[66] I. Mora-Sero, T. Dittrich, G. Garcia-Belmonte, J. Bisquert, J. Appl. Phys. 100 (2006) 103705.
[67] D. Xu, T. Jiang, D. Wang, L. Chen, L. Zhang, Z. Fu, L. Wang, T. Xie, Acs Appl. Mater. Inter. 6 (2014) 9321–9327.
[68] X. Zou, P.-P. Wang, C. Li, J. Zhao, D. Wang, T. Asefa, G.-D. Li, J. Mater. Chem. A 2 (2014) 4682–4689.
[69] Y.C. Lu, L.L. Wang, D.J. Wang, T.F. Xie, L.P. Chen, Y.H. Lin, Mater. Chem. Phys. 129 (2011) 281–287.
[70] Q. Zhao, T. Xie, L. Peng, Y. Lin, P. Wang, L. Peng, D. Wang, J. Phys. Chem. C 111 (2007) 17136–17145.
[71] L. Shi, L. Liang, F. Wang, M. Liu, J. Sun, RSC Adv. 5 (2015) 101843–101849.
[72] Q. Liu, T.X. Chen, Y.R. Guo, Z.G. Zhang, X.M. Fang, Appl. Catal. B-Environ. 193 (2016) 248–258.
[73] J.-X. Sun, Y.-P. Yuan, L.-G. Qiu, X. Jiang, A.-J. Xie, Y.-H. Shen, J.-F. Zhu, Dalton Trans. 41 (2012) 6756–6763.
[74] R. Marschall, L. Wang, Catal. Today 225 (2014) 111–135.
[75] C. Zhou, L. Shang, H. Yu, T. Bian, L.-Z. Wu, C.-H. Tung, T. Zhang, Catal. Today 225 (2014) 158–163.
[76] C. Zhen, R. Chen, L. Wang, G. Liu, H.-M. Cheng, J. Mater. Chem. A 4 (2016) 2783–2800.
[77] K. Sasan, F. Zuo, Y. Wang, P. Feng, Nanoscale 7 (2015) 13369–13372.
[78] G. Li, Z. Lian, X. Li, Y. Xu, W. Wang, D. Zhang, F. Tian, H. Li, J. Mater. Chem. A 3 (2015) 3748–3756.
[79] F. Zuo, L. Wang, T. Wu, Z. Zhang, D. Borchardt, P. Feng, J. Am. Chem. Soc. 132 (2010) 11856–11857.
[80] J. Zhang, L. Li, Z. Xiao, D. Liu, S. Wang, J. Zhang, Y. Hao, W. Zhang, ACS Sustain. Chem. Eng. 4 (2016) 2037–2046.
[81] S.G. Ullattil, P. Periyat, J. Mater. Chem. A 4 (2016) 5854–5858.